Int J Adv Manuf Technol (2015) 77:1793–1809
DOI 10.1007/s00170-014-6550-8

ORIGINAL ARTICLE

A prediction method of cutting force coefficients with helix angle of flat-end cutter and its application in a virtual three-axis milling simulation system

Yung-Chou Kao · Nhu-Tung Nguyen · Mau-Sheng Chen · Shin-Tzong Su

Received: 5 June 2014 / Accepted: 27 October 2014 / Published online: 19 November 2014

Abstract Predicting the quality of a machined component is the grandiose signification in manufacturing industry. Calculation of the cutting force is one of the most important elements to predict the quality of machined parts. In this paper, a linear force model is developed in which the cutter's helix angle is incorporated to calculate the cutting force coefficients for the milling process. On the effect of cutter's helix angle, all derivations of cutting forces are directly based on the tangential, radial, and axial cutting force components. In the developed mathematical model, with the stable milling condition, the average cutting forces are expressed as a linear function of the feedrate, and the cutting force coefficient model is formulated by a function of average cutting force and cutter geometry such as cutter diameter, number of flutes, cutter's helix angle. An experimental method is proposed based on the stable milling condition to estimate the cutting force coefficients. This method can be applied to each pair of cutter and workpiece. The developed cutting force calculation model has been successfully verified by both simulation and experiment with very promising results. Integrated application with a virtual three-axis milling machining simulation system has also been implemented to demonstrate potential utilization of this developed model.

Keywords Cylindrical flat-end mill · Cutting force · Cutting force coefficients · Cutting force simulation

Y.-C. Kao · N.-T. Nguyen (✉) · M.-S. Chen · S.-T. Su
Department of Mechanical Engineering, National Kaohsiung University of Applied Sciences, 415 Chien Kung Road, Sanmin District, Kaohsiung 80778, Taiwan, Republic of China
e-mail: tungdhhv@gmail.com

Nomenclature

D	The diameter of cutter [mm]
N_f	The number of flutes on the cutter
β	The helix angle on the cutter [deg]
ϕ_p	The cutter pitch angle [deg]
Ψ	The lag angle at an axial depth of cut z [deg]
Ψ_a	The lag angle at maximum axial depth of cut z=a [deg]
ϕ_j	The instantaneous immersion angle of flute number j, (j=1~N_f) [deg]
ϕ_{st}	The cutter entry angle [deg]
ϕ_{ex}	The cutter exit angle [deg]
f_t	The feed per tooth [mm/tooth]
$h_j(\phi_j(z))$	The instantaneous chip thickness at immersion angle ϕ_j [mm]
a	The full axial depth of cut [mm]
dz	The differential axial depth of cut [mm]
$z_{j,1}$	The lower axial engagement limit of the in-cut portion for the flute number j [mm]
$z_{j,2}$	The upper axial engagement limit of the in-cut portion for the flute number j, [mm]
K_{tc}	Tangential shearing force coefficient [N/mm^2]
K_{rc}	Radial shearing force coefficient [N/mm^2]
K_{ac}	Axial shearing force coefficient [N/mm^2]
K_{te}	Tangential edge force coefficient [N/mm]

K_{re}	Radial edge force coefficient [N/mm]
K_{ae}	Axial edge force coefficient [N/mm]
$dF_{t,j}(\phi, z)$	The differential tangential cutting force [N]
$dF_{r,j}(\phi, z)$	The differential radial cutting force [N]
$dF_{a,j}(\phi, z)$	The differential axial cutting force [N]
$dF_{f,j}(\phi, z)$	The differential feed cutting force [N]
$dF_{n,j}(\phi, z)$	The differential normal cutting force [N]
$F_f(\phi)$	The cutting force in the feed direction [N]
$F_n(\phi)$	The cutting force in the normal direction [N]
$F_a(\phi)$	The cutting force in the axial direction [N]
$\overline{F}_f$	The average cutting force in the feed direction [N]
$\overline{F}_{fc}$, $\overline{F}_{fe}$	The components of linear model force in the feed direction [N]
$\overline{F}_n$	The average cutting force in the normal direction [N]
$\overline{F}_{nc}$, $\overline{F}_{ne}$	The components of linear model force in the normal direction [N]
$\overline{F}_a$	The average cutting force in the axial direction [N]
$\overline{F}_{ac}$, $\overline{F}_{ae}$	The components of linear model force in the axial direction [N]
θ	The angle between feed and x direction [deg]
$A_q(Max)$	The maximum cutting force's amplitude [N] (q=f, n, a)
$A_q(Min)$	The minimum cutting force's amplitude [N]
Δ_q	The degree of variation of force's amplitude [%]
F_x	The cutting force in x direction [N]
F_y	The cutting force in y direction [N]
F_z	The cutting force in z direction [N]

1 Introduction

Milling is not only the most common processes in machining, but also is very popularly employed in computer numerical control (CNC) machines for metal material removal operations. Reliable quantitative prediction of cutting force coefficients and cutting forces in milling is very important to predict the power and torque requirements, machine tool vibrations, surface quality, geometrical accuracy, and stability, etc. However, in view of power, surface quality, productivity, and stability are limited by milling process defectiveness, such as deflection and chatter regeneration resulted from cutting forces.

Metal-cutting mechanics can be analyzed by orthogonal and oblique models although almost all practical cutting processes are oblique cutting processes. Mechanics of orthogonal and oblique cutting have been investigated in many works such as Merchant [1] and Altintas [2]. Although the formulations of the process mechanics in many of these research are similar, there are significant differences in the approach used in implementing the models to predict the cutting forces in practical processes. The procedure of cutting force modeling is generally realized by developing the experiential chip-force relationship through cutting force coefficients, and the accuracy of cutting force coefficient's prediction largely affects the prediction accuracy of cutting forces. Thus, effective methods for calibrating the cutting coefficients are the important keys to cutting force's modeling.

In the traditional mechanistic approach, edge force and shear force coefficients are calibrated for different pairs of the workpiece and tool through the cutting tests, which has been used for turning, drilling, and milling operations [2–4]. The reviews of these studies showed that there existed two typical methods for the calibration of cutting force coefficients. The first method is the orthogonal to oblique cutting transformation method, and the second method is the direct calibration method.

In the first method, the shear angle, friction angle, and shear yield stress resulted from orthogonal cutting test were used to estimate the cutting force coefficients. Following this approach, the cutting force coefficients were determined using the oblique cutting model, the orthogonal model, and the cutting data [2, 5, 6]. On the other hand, the cutting force coefficients were calculated from the oblique cutting model with and without end cutting edge effect and tool nose radius effect [7]. Furthermore, by this way, some researchers developed models to calculate cutting force coefficients that could be applied for ball-end milling using the data from orthogonal cutting tests [8–10].

In the second method, the cutting force coefficients were determined directly from milling tests for the specific cutter part combination. Cheng et al. [11] determined the instantaneous cutting force coefficients in terms of the instantaneous uncut chip thickness, the cutting edge length, and the spindle speed. Bayoumi et al. [12] determined the instantaneous cutting force coefficients by considering the instantaneous uncut chip thickness and the cutter rake angle simultaneously. Shin and Waters [13] developed a model to estimate the instantaneous cutting force coefficients with an improved simulation model of chip flow angle. Larue and Anselmetti [14] used the measurement of cutter deflection to determine the cutting force coefficients. Azeem et al. [15] proposed a systematic method to estimate the cutting force coefficients and the cutter runout parameters for a two-flute ball-end mill by considering the instantaneous cutting force. Ko and Cho [16] determined the cutting force coefficients by using the relationship between the instantaneous uncut chip thickness and the instantaneous cutting force. Subrahmanyam et al. [17] used the corresponding maximum chip area and maximum measured force to estimate the cutting force coefficients, whereas Altintas [2, 18], Budak [19], Adetoro and Wen [20], Wang et al. [21], Compeán et al. [22], and Wan et al. [23] calculated the cutting force coefficients by using the measured average cutting forces.

With direct calibration method, two models often are used to calculate the cutting force coefficients. In the first one, the effect of shearing mechanism due to chip generating process on the rake face and the effects of rubbing and ploughing mechanisms on the flank face of the tool are lumped into one specific cutting force coefficients for each cutting force component (tangential, radial, and axial); so, the cutting force coefficients are relatively dependent on the average chip thickness (exponential force coefficient model). This model is quite complex to analyze and to calculate [24–29]. In the second model, the effect of the shearing and ploughing mechanism is characterized separately by the specific and edge force coefficients, respectively. In this case, the cutting force coefficients are relatively independent of the average chip thickness (linear force model) [2, 19, 21, 30]. This model is quite suitable to be applied to many types of milling tool such as flat-end mill [2, 18, 19, 21], ball-end mill [31, 32], bull-end mill [33], and general-end mill [34]. However, when determining the cutting force coefficient in milling, it seems that the previous studies were simplified without the effect of cutter's helix angle; so, some cutting force coefficients were neglected and are called the simplified models.

This study researches and verifies the linear force model in the flat-end mill. The shear and edge force coefficients are determined from the experimental data of average cutting forces. The developed model could be used for estimation of the cutting force coefficients. The main contributions of this study lie in four aspects: (1) The theory formulas to calculate the cutting force coefficients were built with the effect of cutter's helix angle, (2) an experimental method was investigated to determine the stable cutting condition and estimate the cutting force coefficients, and (3) by experimental method, all cutting force coefficients were determined by experimental data of average cutting forces. Moreover, (4) the integrated application with a virtual three-axis milling machining simulation system has also been implemented to demonstrate potential utilization of this research showing very promising application.

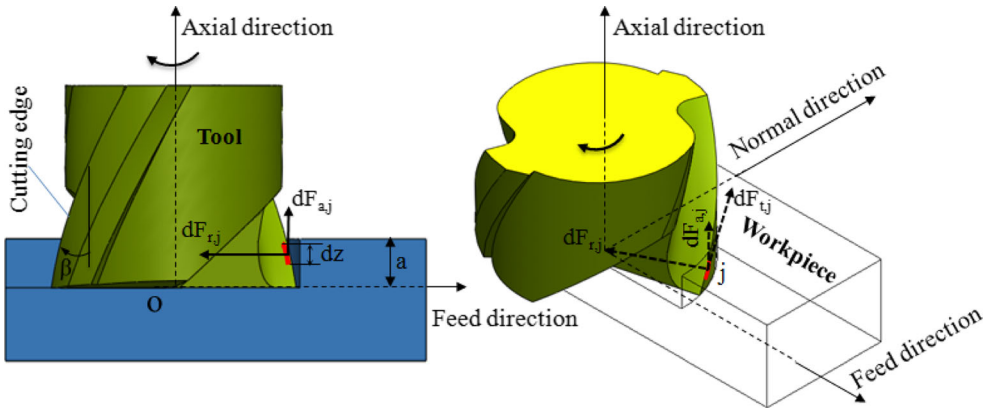

Fig. 1 Geometry of cylindrical end-mill

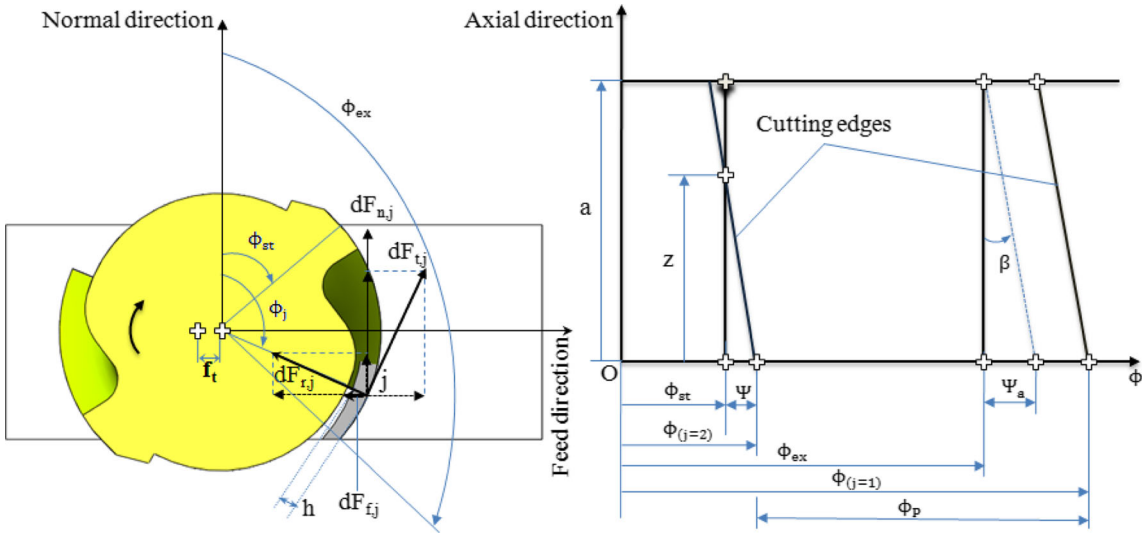

Fig. 2 The angular position of the cutter's flute

2 Mathematics of cutting force model for cylindrical flat-end mill

2.1 The mathematics cutting force model

In cylindrical flat-end mill, as shown in Figs. 1 and 2, the immersion is measured clockwise from the normal axis. Assuming that the bottom end of flute number one is designated as the reference immersion angle (ϕ_1) and the bottom end point of the remaining flute number j is at an angle (ϕ_j), then ϕ_j can be expressed as in Eq. 1.

$$\Phi_j = \Phi_1 - (j-1)\Phi_P, \quad j = 1 \sim N_f \tag{1}$$

where ϕ_P is the cutter pitch angle that is the lag angle from the flute number j to the flute number j+1.

$$\Phi_P = \frac{2\pi}{N_f} \tag{2}$$

When considering the cutter's helix angle, the lag angle "Ψ" at each axial depth of cut z can be expressed in Eq. 3 [2].

$$\Psi = \frac{2\tan\beta}{D} z \tag{3}$$

For flute number j, at an axial depth of cut z, the immersion angle is $\phi_j(z)$. It can be expressed by Eq. 4, as shown in Fig. 2.

$$\Phi_j(z) = \Phi_j - \Psi = \Phi_1 - (j-1)\Phi_P - \Psi = \Phi_1 - (j-1)\Phi_P - \frac{2\tan\beta}{D} z \tag{4}$$

If zero nose radius of the cutter is assumed, the tangential, radial, and axial forces acting on a differential flute element can be expressed as in Eq. 5 [2].

$$\begin{cases} dF_{t,j}(\Phi, z) = K_{te} * dz + K_{tc} * h_j\left(\Phi_j(z)\right) * dz \\ dF_{r,j}(\Phi, z) = K_{re} * dz + K_{rc} * h_j\left(\Phi_j(z)\right) * dz \\ dF_{a,j}(\Phi, z) = K_{ae} * dz + K_{ac} * h_j\left(\Phi_j(z)\right) * dz \end{cases} \tag{5}$$

where the instantaneous chip thickness $h_j\left(\phi_j(z)\right)$ is determined by Eq. 6 [2].

$$h_j\left(\Phi_j(z)\right) = f_t \sin\Phi_j(z) \tag{6}$$

From Eqs. 5 to 6, the components of cutting forces can be calculated by Eq. 7.

$$\begin{cases} dF_{t,j}(\Phi, z) = \left[K_{tc} f_t \sin\Phi_j(z) + K_{te}\right] * dz \\ dF_{r,j}(\Phi, z) = \left[K_{rc} f_t \sin\Phi_j(z) + K_{re}\right] * dz \\ dF_{a,j}(\Phi, z) = \left[K_{ac} f_t \sin\Phi_j(z) + K_{ae}\right] * dz \end{cases} \tag{7}$$

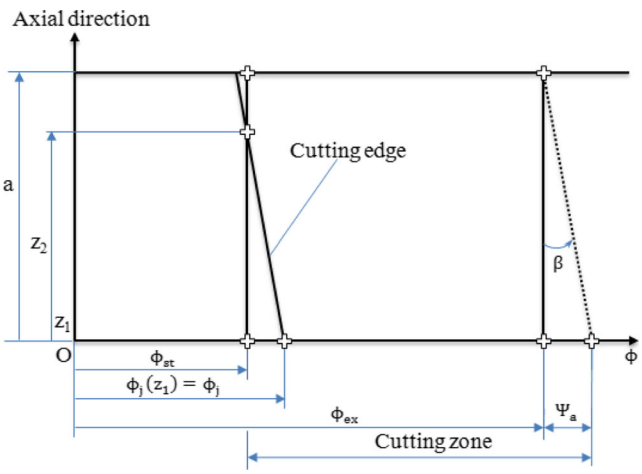

Fig. 3 The boundary conditions

In Figs. 1 and 2, each point at cutting edge is determined by z coordinate and the angular position ϕ_j (). In those points, the cutting forces consist of three components including radial force, tangential force, and axial force. The feed direction is the direction that is parallel to the tool movement direction, and perpendicular to the tool axis. The normal direction is perpendicular to the tool movement direction and tool axis. The axial direction is parallel to the tool axis and perpendicular to the tool path. So, the elemental forces in feed, normal, and axial force are calculated by using the transformation as in Eq. 8

$$\begin{Bmatrix} dF_{f,j}(\phi,z) \\ dF_{n,j}(\phi,z) \\ dF_{a,j}(\phi,z) \end{Bmatrix} = \begin{bmatrix} -\cos\phi_j(z) & -\sin\phi_j(z) & 0 \\ \sin\phi_j(z) & -\cos\phi_j(z) & 0 \\ 0 & 0 & 1 \end{bmatrix} \begin{Bmatrix} dF_{t,j}(\phi,z) \\ dF_{r,j}(\phi,z) \\ dF_{a,j}(\phi,z) \end{Bmatrix} \tag{8}$$

So

$$\begin{cases} dF_{f,j}(\phi,z) = -\left[K_{tc}\, f_t \sin\phi_j(z) + K_{te}\right] dz \cos\phi_j(z) - \left[K_{rc}\, f_t \sin\phi_j(z) + K_{re}\right] dz \sin\phi_j(z) \\ dF_{n,j}(\phi,z) = \left[K_{tc}\, f_t \sin\phi_j(z) + K_{te}\right] dz \sin\phi_j(z) - \left[K_{rc}\, f_t \sin\phi_j(z) + K_{re}\right] dz \cos\phi_j(z) \\ dF_{a,j}(\phi,z) = \left[K_{ac}\, f_t \sin\phi_j(z) + K_{ae}\right] dz \end{cases} \tag{9}$$

and

$$\begin{cases} dF_{f,j}(\phi,z) = \left\{ \dfrac{f_t}{2}\left[-K_{tc}\sin 2\phi_j(z) - K_{rc}\left(1-\cos 2\phi_j(z)\right)\right] + \left[-K_{te}\cos\phi_j(z) - K_{re}\sin\phi_j(z)\right] \right\} dz \\ dF_{n,j}(\phi,z) = \left\{ \dfrac{f_t}{2}\left[K_{tc}\left(1-\cos 2\phi_j(z)\right) - K_{rc}\sin 2\phi_j(z)\right] + \left[K_{te}\sin\phi_j(z) - K_{re}\cos\phi_j(z)\right] \right\} dz \\ dF_{a,j}(\phi,z) = \left[K_{ac}\, f_t \sin\phi_j(z) + K_{ae}\right] dz \end{cases} \tag{10}$$

In the determination of the total cutting force, the differential cutting forces are integrated analytically along the in-cut portion of the flute j, Eq. 11.

$$F_q(\phi_j(z)) = F_q(\phi,z) = \int_{z_{j,1}}^{z_{j,2}} dF_q(\phi,z), \quad q = f,\ n,\ a \tag{11}$$

2.1.1 Using the integration by change of variable

The values $z_{j,1}$ and $z_{j,2}$ are the lower and upper axial engagement limits of the in-cut portion for the flute number j. The change of variable is used as in Eqs. 12 and 13.

$$\phi_j(z) = \phi_1 - (j-1)\phi_P - \frac{2\tan\beta}{D} z \Rightarrow d\phi_j(z) = -\frac{2\tan\beta}{D} dz \tag{12}$$

so

$$dz = -\frac{D}{2\tan\beta} d\phi_j(z), \text{ and } \begin{cases} z = z_{j,1} \Rightarrow \phi_j(z) = \phi_j(z_1) \\ z = z_{j,2} \Rightarrow \phi_j(z) = \phi_j(z_2) \end{cases} \tag{13}$$

Combining Eqs. 11 to 14, the cutting forces can be calculated by Eqs. 14 to 16.

$$F_q(\phi_j(z)) = -\frac{D}{2\tan\beta} \int_{\phi_j(z_1)}^{\phi_j(z_2)} dF_q\left(\phi_j(z)\right), \quad q = f,\ n,\ a \tag{14}$$

or

$$\begin{cases} F_{f,j}(\phi(z)) = -\dfrac{D}{2\tan\beta} \displaystyle\int_{\phi_j(z_1)}^{\phi_j(z_2)} \left\{ \dfrac{f_t}{2}\left[-K_{tc}\sin 2\phi_j(z) - K_{rc}\left(1-\cos 2\phi_j(z)\right)\right] + \left[-K_{te}\cos\phi_j(z) - K_{re}\sin\phi_j(z)\right] \right\} d\phi \\ F_{n,j}(\phi(z)) = -\dfrac{D}{2\tan\beta} \displaystyle\int_{\phi_j(z_1)}^{\phi_j(z_2)} \left\{ \dfrac{f_t}{2}\left[K_{tc}\left(1-\cos 2\phi_j(z)\right) - K_{rc}\sin 2\phi_j(z)\right] + \left[K_{te}\sin\phi_j(z) - K_{re}\cos\phi_j(z)\right] \right\} d\phi \\ F_{a,j}(\phi(z)) = -\dfrac{D}{2\tan\beta} \displaystyle\int_{\phi_j(z_1)}^{\phi_j(z_2)} \left\{ K_{ac}\, f_t \sin\phi_j(z) + K_{ae} \right\} d\phi \end{cases} \tag{15}$$

so

$$\begin{cases} F_{f,j}(\phi(z)) = \left\{ -\frac{Df_t}{8\tan\beta}\left[K_{tc}\cos 2\phi_j(z) - K_{rc}\left(2\phi_j(z) - \sin 2\phi_j(z)\right)\right] + \frac{D}{2\tan\beta}\left[K_{te}\sin\phi_j(z) - K_{re}\cos\phi_j(z)\right] \right\}_{\phi_j(z_1)}^{\phi_j(z_2)} \\ F_{n,j}(\phi(z)) = \left\{ -\frac{Df_t}{8\tan\beta}\left[K_{tc}\left(2\phi_j(z) - \sin 2\phi_j(z)\right) - K_{rc}\cos 2\phi_j(z)\right] + \frac{D}{2\tan\beta}\left[K_{te}\cos\phi_j(z) + K_{re}\sin\phi_j(z)\right] \right\}_{\phi_j(z_1)}^{\phi_j(z_2)} \\ F_{a,j}(\phi(z)) = \left\{ \frac{Df_t}{2\tan\beta}\left[K_{ac}\cos\phi_j(z) + \frac{D}{2\tan\beta}K_{ae}\phi_j(z)\right] \right\}_{\phi_j(z_1)}^{\phi_j(z_2)} \end{cases} \quad (16)$$

Considering the case that has more than one tooth executing the cutting processes simultaneously, the total cutting forces on the feed, normal, and axial direction can be determined by Eq. 17.

$$F_f(\phi) = \sum_{j=1}^{N_f} F_{f,j}(\phi_j), \quad F_n(\phi) = \sum_{j=1}^{N_f} F_{n,j}(\phi_j), \quad F_a(\phi) = \sum_{j=1}^{N_f} F_{a,j}(\phi_j) \quad (17)$$

2.1.2 Determine the boundary conditions

The lag angle at full axial depth of cut is calculated by Eq. 18 [2].

$$\Psi_a = \frac{2\tan\beta}{D}a \quad (18)$$

The cutting forces exist only when the cutting tool is in the cutting zone, as shown in Fig. 3, and can be expressed in Eq. 19.

$$\phi_{st} \le \phi_j \le \phi_{ex} + \Psi_a \quad (19)$$

In each revolution, the boundary conditions for calculation of cutting forces are illustrated as in Fig. 3 and can be expressed in Eq. 20.

$$\begin{cases} \text{If } (\phi_j < \phi_{st}) \text{ or } (\phi_j > \phi_{ex} + \Psi_a) \Rightarrow \text{Out of cut}: \ F_{(f,n,a)}(j) = 0 \\ \text{If } (\phi_{st} \le \phi_j < \phi_{st} + \Psi_a) \Rightarrow \text{cutting} \begin{cases} \phi_j(z_1) = \phi_j \\ \phi_j(z_2) = \phi_{st} \end{cases} \\ \text{If } (\phi_{st} + \Psi_a \le \phi_j < \phi_{ex}) \Rightarrow \text{cutting} \begin{cases} \phi_j(z_1) = \phi_j \\ \phi_j(z_2) = \phi_j - \Psi_a \end{cases} \\ \text{If } (\phi_{ex} \le \phi_j \le \phi_{ex} + \Psi_a) \Rightarrow \text{cutting} \begin{cases} \phi_j(z_1) = \phi_j \\ \phi_j(z_2) = \phi_{ex} \end{cases} \end{cases} \quad (20)$$

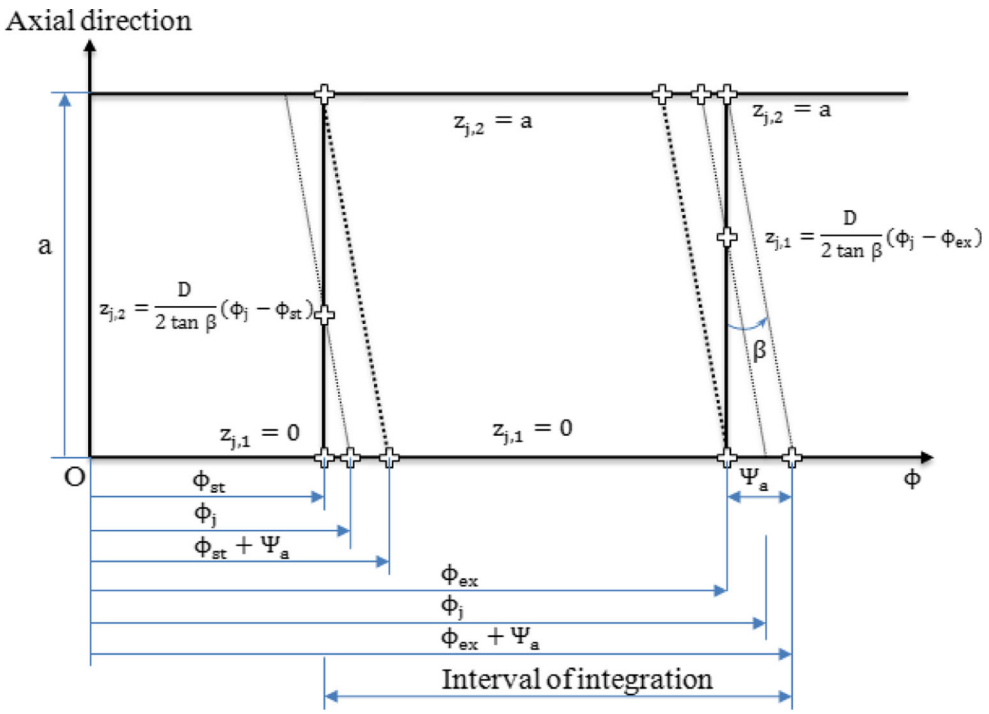

Fig. 4 Interval of integration

2.2 Identification of cutting force coefficients

The average cutting forces of N_f flutes per revolution can be expressed by Eq. 21.

$$\begin{cases} F_f = \dfrac{N_f}{2\pi}\displaystyle\int_{\phi_{st}}^{\phi_{ex}+\Psi_a}\left(\int_{z_{j,1}}^{z_{j,2}} dF_{f,j}(\phi(z))\right)d\phi \\ F_n = \dfrac{N_f}{2\pi}\displaystyle\int_{\phi_{st}}^{\phi_{ex}+\Psi_a}\left(\int_{z_{j,1}}^{z_{j,2}} dF_{n,j}(\phi(z))\right)d\phi \\ F_a = \dfrac{N_f}{2\pi}\displaystyle\int_{\phi_{st}}^{\phi_{ex}+\Psi_a}\left(\int_{z_{j,1}}^{z_{j,2}} dF_{a,j}(\phi(z))\right)d\phi \end{cases} \quad (21)$$

In the Eq. 21, the integration interval was separated by three subintervals. The first one are values from ϕ_{st} to $\phi_{st}+\Psi_a$, the second one are values from $(\phi_{st}+\Psi_a)$ to ϕ_{ex}, and the third subinterval are values from (ϕ_{ex}) to $(\phi_{ex}+\Psi_a)$ as shown in Fig. 4; so, Eq. 21 becomes Eq. 22.

$$\begin{cases} F_f = \dfrac{N_f}{2\pi}\left[\displaystyle\int_{\phi_{st}}^{\phi_{st}+\Psi_a}\left(\int_{z_{j,1}}^{z_{j,2}} dF_{f,j}(\phi(z))\right)d\phi + \int_{\phi_{st}+\Psi_a}^{\phi_{ex}}\left(\int_{z_{j,1}}^{z_{j,2}} dF_{f,j}(\phi(z))\right)d\phi + \int_{\phi_{ex}}^{\phi_{ex}+\Psi_a}\left(\int_{z_{j,1}}^{z_{j,2}} dF_{f,j}(\phi(z))\right)d\phi\right] \\ F_n = \dfrac{N_f}{2\pi}\left[\displaystyle\int_{\phi_{st}}^{\phi_{st}+\Psi_a}\left(\int_{z_{j,1}}^{z_{j,2}} dF_{n,j}(\phi(z))\right)d\phi + \int_{\phi_{st}+\Psi_a}^{\phi_{ex}}\left(\int_{z_{j,1}}^{z_{j,2}} dF_{n,j}(\phi(z))\right)d\phi + \int_{\phi_{ex}}^{\phi_{ex}+\Psi_a}\left(\int_{z_{j,1}}^{z_{j,2}} dF_{n,j}(\phi(z))\right)d\phi\right] \\ F_a = \dfrac{N_f}{2\pi}\left[\displaystyle\int_{\phi_{st}}^{\phi_{st}+\Psi_a}\left(\int_{z_{j,1}}^{z_{j,2}} dF_{a,j}(\phi(z))\right)d\phi + \int_{\phi_{st}+\Psi_a}^{\phi_{ex}}\left(\int_{z_{j,1}}^{z_{j,2}} dF_{a,j}(\phi(z))\right)d\phi + \int_{\phi_{ex}}^{\phi_{ex}+\Psi_a}\left(\int_{z_{j,1}}^{z_{j,2}} dF_{a,j}(\phi(z))\right)d\phi\right] \end{cases} \quad (22)$$

The axial integration boundaries are shown in Fig. 4. If the angular position of cutting edge is in the first subinterval (from ϕ_{st} to $\phi_{st}+\Psi_a$), the values for integration limits will be $z_{j,1}=0$ and $z_{j,2}=\frac{D}{2\tan\beta}\left(\phi_j-\phi_{st}\right)$. If the angular position of cutting edge is in the second subinterval (from $\phi_{st}+\Psi_a$ to ϕ_{ex}), the values for integration limits will be $z_{j,1}=0$ and $z_{j,2}=a$. If it is in the third subinterval (from ϕ_{ex} to $\phi_{ex}+\Psi_a$), the values for integration limits will be $z_{j,1}=\frac{D}{2\tan\beta}\left(\phi_j-\phi_{ex}\right)$ and $z_{j,2}=a$; so, the average cutting forces are determined by Eqs. 23 to 25.

In feed direction

$$\overline{F}_f = \begin{cases} \dfrac{N_f}{4\pi}K_{tc}f_t\left(-\displaystyle\int_{\phi_{st}}^{\phi_{st}+\Psi_a}\left[\int_0^{\frac{D}{2\pi}(\phi-\phi_{st})}\left(\sin2\phi_j(z)\right)dz\right]d\phi-\int_{\phi_{st}+\Psi_a}^{\phi_{ex}}\left[\int_0^{a}\left(\sin2\phi_j(z)\right)dz\right]d\phi-\int_{\phi_{ex}}^{\phi_{ex}+\Psi_a}\left[\int_{\frac{D}{2\pi}(\phi-\phi_{ex})}^{a}\left(\sin2\phi_j(z)\right)dz\right]d\phi\right) \\ +\dfrac{N_f}{4\pi}K_{rc}f_t\left(-\displaystyle\int_{\phi_{st}}^{\phi_{st}+\Psi_a}\left[\int_0^{\frac{D}{2\pi}(\phi-\phi_{st})}\left(1-\cos2\phi_j(z)\right)dz\right]d\phi-\int_{\phi_{st}+\Psi_a}^{\phi_{ex}}\left[\int_0^{a}\left(1-\cos2\phi_j(z)\right)dz\right]d\phi-\int_{\phi_{ex}}^{\phi_{ex}+\Psi_a}\left[\int_{\frac{D}{2\pi}(\phi-\phi_{ex})}^{a}\left(1-\cos2\phi_j(z)\right)dz\right]d\phi\right) \\ +\dfrac{N_f}{2\pi}K_{te}\left(-\displaystyle\int_{\phi_{st}}^{\phi_{st}+\Psi_a}\left[\int_0^{\frac{D}{2\pi}(\phi-\phi_{st})}\left(\cos\phi_j(z)\right)dz\right]d\phi-\int_{\phi_{st}+\Psi_a}^{\phi_{ex}}\left[\int_0^{a}\left(\cos\phi_j(z)\right)dz\right]d\phi-\int_{\phi_{ex}}^{\phi_{ex}+\Psi_a}\left[\int_{\frac{D}{2\pi}(\phi-\phi_{ex})}^{a}\left(\cos\phi_j(z)\right)dz\right]d\phi\right) \\ +\dfrac{N_f}{2\pi}K_{re}\left(-\displaystyle\int_{\phi_{st}}^{\phi_{st}+\Psi_a}\left[\int_0^{\frac{D}{2\pi}(\phi-\phi_{st})}\left(\sin\phi_j(z)\right)dz\right]d\phi-\int_{\phi_{st}+\Psi_a}^{\phi_{ex}}\left[\int_0^{a}\left(\sin\phi_j(z)\right)dz\right]d\phi-\int_{\phi_{ex}}^{\phi_{ex}+\Psi_a}\left[\int_{\frac{D}{2\pi}(\phi-\phi_{ex})}^{a}\left(\sin\phi_j(z)\right)dz\right]d\phi\right) \end{cases} \quad (23)$$

In normal direction

$$\overline{F}_n = \left\{ \begin{array}{l} \frac{N_f}{4\pi} K_{tc} f_t \left(-\int_{\phi_{st}}^{\phi_{st}+\Psi_a} \left[\int_0^{\frac{D}{2\pi}(\phi-\phi_{st})} \left(1-\cos 2\phi_j(z)\right) dz \right] d\phi + \int_{\phi_{st}+\Psi_a}^{\phi_{ex}} \left[\int_0^a \left(1-\cos 2\phi_j(z)\right) dz \right] d\phi - \int_{\phi_{ex}}^{\phi_{ex}+\Psi_a} \left[\int_{\frac{D}{2\pi}(\phi-\phi_{ex})}^a \left(1-\cos 2\phi_j(z)\right) dz \right] d\phi \right) \\ + \frac{N_f}{4\pi} K_{rc} f_t \left(-\int_{\phi_{st}}^{\phi_{st}+\Psi_a} \left[\int_0^{\frac{D}{2\pi}(\phi-\phi_{st})} \left(\sin 2\phi_j(z)\right) dz \right] d\phi - \int_{\phi_{st}+\Psi_a}^{\phi_{ex}} \left[\int_0^a \left(\sin 2\phi_j(z)\right) dz \right] d\phi - \int_{\phi_{ex}}^{\phi_{ex}+\Psi_a} \left[\int_{\frac{D}{2\pi}(\phi-\phi_{ex})}^a \left(\sin 2\phi_j(z)\right) dz \right] d\phi \right) \\ + \frac{N_f}{2\pi} K_{te} \left(\int_{\phi_{st}}^{\phi_{st}+\Psi_a} \left[\int_0^{\frac{D}{2\pi}(\phi-\phi_{st})} \left(\sin \phi_j(z)\right) dz \right] d\phi + \int_{\phi_{st}+\Psi_a}^{\phi_{ex}} \left[\int_0^a \left(\sin \phi_j(z)\right) dz \right] d\phi + \int_{\phi_{ex}}^{\phi_{ex}+\Psi_a} \left[\int_{\frac{D}{2\pi}(\phi-\phi_{ex})}^a \left(\sin \phi_j(z)\right) dz \right] d\phi \right) \\ + \frac{N_f}{2\pi} K_{re} \left(-\int_{\phi_{st}}^{\phi_{st}+\Psi_a} \left[\int_0^{\frac{D}{2\pi}(\phi-\phi_{st})} \left(\cos \phi_j(z)\right) dz \right] d\phi - \int_{\phi_{st}+\Psi_a}^{\phi_{ex}} \left[\int_0^a \left(\cos \phi_j(z)\right) dz \right] d\phi - \int_{\phi_{ex}}^{\phi_{ex}+\Psi_a} \left[\int_{\frac{D}{2\pi}(\phi-\phi_{ex})}^a \left(\cos \phi_j(z)\right) dz \right] d\phi \right) \end{array} \right\} \tag{24}$$

In axial direction

$$\overline{F}_a \left\{ \begin{array}{l} \frac{N_f}{2\pi} K_{ac} f_t \left(\int_{\phi_{st}}^{\phi_{st}+\Psi_a} \left[\int_0^{\frac{D}{2\pi}(\phi-\phi_{st})} \left(\sin \phi_j(z)\right) dz \right] d\phi + \int_{\phi_{st}+\Psi_a}^{\phi_{ex}} \left[\int_0^a \left(\sin \phi_j(z)\right) dz \right] d\phi + \int_{\phi_{ex}}^{\phi_{ex}+\Psi_a} \left[\int_{\frac{D}{2\pi}(\phi-\phi_{ex})}^a \left(\sin \phi_j(z)\right) dz \right] d\phi \right) \\ + \frac{N_f}{2\pi} K_{ae} \left(\int_{\phi_{st}}^{\phi_{st}+\Psi_a} \left[\int_0^{\frac{D}{2\pi}(\phi-\phi_{st})} dz \right] d\phi + \int_{\phi_{st}+\Psi_a}^{\phi_{ex}} \left[\int_0^a dz \right] d\phi + \int_{\phi_{ex}}^{\phi_{ex}+\Psi_a} \left[\int_{\frac{D}{2\pi}(\phi-\phi_{ex})}^a dz \right] d\phi \right) \end{array} \right\} \tag{25}$$

Setting

$$\left\{ \begin{array}{l} C_1 = \frac{N_f}{4\pi} \left(-\int_{\phi_{st}}^{\phi_{st}+\Psi_a} \left[\int_0^{\frac{D}{2\pi}(\phi-\phi_{st})} \left(\sin 2\phi_j(z)\right) dz \right] d\phi - \int_{\phi_{st}+\Psi_a}^{\phi_{ex}} \left[\int_0^a \left(\sin 2\phi_j(z)\right) dz \right] d\phi - \int_{\phi_{ex}}^{\phi_{ex}+\Psi_a} \left[\int_{\frac{D}{2\pi}(\phi-\phi_{ex})}^a \left(\sin 2\phi_j(z)\right) dz \right] d\phi \right) \\ C_2 = \frac{N_f}{4\pi} \left(-\int_{\phi_{st}}^{\phi_{st}+\Psi_a} \left[\int_0^{\frac{D}{2\pi}(\phi-\phi_{st})} \left(1-\cos 2\phi_j(z)\right) dz \right] d\phi - \int_{\phi_{st}+\Psi_a}^{\phi_{ex}} \left[\int_0^a \left(1-\cos 2\phi_j(z)\right) dz \right] d\phi - \int_{\phi_{ex}}^{\phi_{ex}+\Psi_a} \left[\int_{\frac{D}{2\pi}(\phi-\phi_{ex})}^a \left(1-\cos 2\phi_j(z)\right) dz \right] d\phi \right) \\ C_3 = \frac{N_f}{2\pi} \left(-\int_{\phi_{st}}^{\phi_{st}+\Psi_a} \left[\int_0^{\frac{D}{2\pi}(\phi-\phi_{st})} \left(\cos \phi_j(z)\right) dz \right] d\phi - \int_{\phi_{st}+\Psi_a}^{\phi_{ex}} \left[\int_0^a \left(\cos \phi_j(z)\right) dz \right] d\phi - \int_{\phi_{ex}}^{\phi_{ex}+\Psi_a} \left[\int_{\frac{D}{2\pi}(\phi-\phi_{ex})}^a \left(\cos \phi_j(z)\right) dz \right] d\phi \right) \\ C_4 = \frac{N_f}{2\pi} \left(-\int_{\phi_{st}}^{\phi_{st}+\Psi_a} \left[\int_0^{\frac{D}{2\pi}(\phi-\phi_{st})} \left(\sin \phi_j(z)\right) dz \right] d\phi - \int_{\phi_{st}+\Psi_a}^{\phi_{ex}} \left[\int_0^a \left(\sin \phi_j(z)\right) dz \right] d\phi - \int_{\phi_{ex}}^{\phi_{ex}+\Psi_a} \left[\int_{\frac{D}{2\pi}(\phi-\phi_{ex})}^a \left(\sin \phi_j(z)\right) dz \right] d\phi \right) \\ C_5 = \frac{N_f}{2\pi} \left(\int_{\phi_{st}}^{\phi_{st}+\Psi_a} \left[\int_0^{\frac{D}{2\pi}(\phi-\phi_{st})} dz \right] d\phi + \int_{\phi_{st}+\Psi_a}^{\phi_{ex}} \left[\int_0^a dz \right] d\phi + \int_{\phi_{ex}}^{\phi_{ex}+\Psi_a} \left[\int_{\frac{D}{2\pi}(\phi-\phi_{ex})}^a dz \right] d\phi \right) \end{array} \right. \tag{26}$$

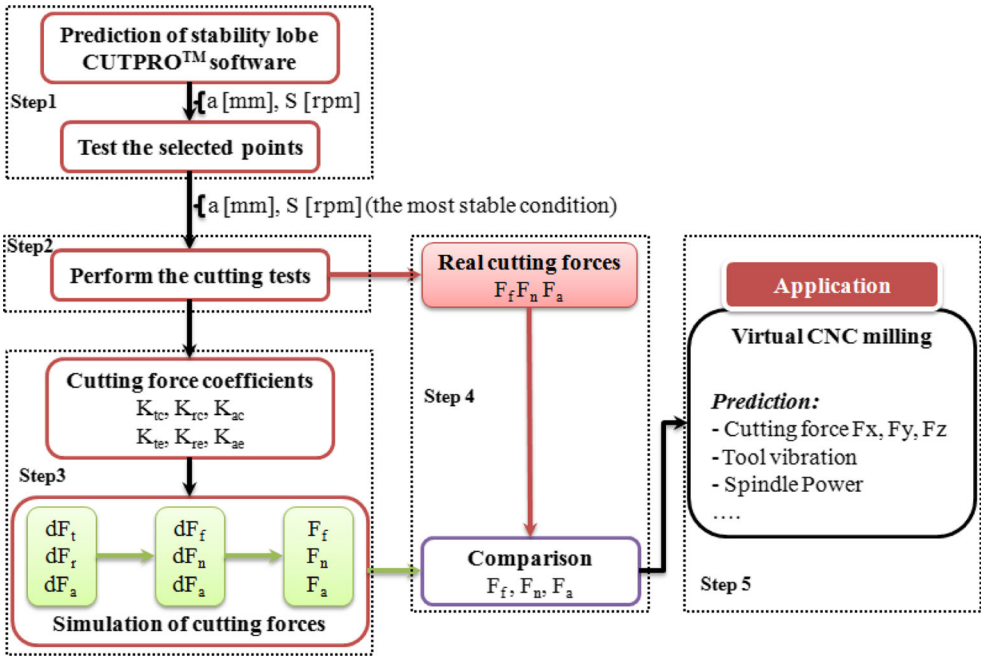

Fig. 5 Approach to determine cutting force coefficients and simulate the cutting forces

Combining Eqs. 23 to 26, the average cutting forces are determined by Eq. 27.

$$\begin{cases} \overline{F}_f = (C_1K_{tc} + C_2K_{rc})\,f_t + C_3K_{te} + C_4K_{re} \\ \overline{F}_n = (-C_2K_{tc} + C_1K_{rc})\,f_t - C_4K_{te} + C_3K_{re} \\ \overline{F}_a = -C_4K_{ac}\,f_t + C_5K_{ae} \end{cases} \tag{27}$$

The average cutting forces can be expressed in Eq. 28, by experimental data.

$$\begin{cases} \overline{F}_f = \overline{F}_{fc}\,f_t + \overline{F}_{fe} \\ \overline{F}_n = \overline{F}_{nc}\,f_t + \overline{F}_{ne} \\ \overline{F}_a = \overline{F}_{ac}\,f_t + \overline{F}_{ae} \end{cases} \tag{28}$$

where the components of the linear force $\overline{F}_{fc}$, $\overline{F}_{fe}$, $\overline{F}_{nc}$, $\overline{F}_{ne}$, $\overline{F}_{ac}$, and $\overline{F}_{ae}$ can be calculated by a linear regression of the measured cutting force data. So, the cutting force coefficients are determined by Eq. 29.

Table 1 Chemical compositions of Al6061-T6

Composite (%)								
Al	Cr	Cu	Fe	Mg	Mn	Si	Ti	Zn
98	≤0.3	≤0.4	≤0.7	≤1.2	≤0.15	≤0.8	≤0.15	≤0.25

$$\begin{cases} K_{tc} = \dfrac{C_1\overline{F}_{fc} - C_2\overline{F}_{nc}}{C_1^2 + C_2^2} & K_{te} = \dfrac{C_3\overline{F}_{fe} - C_4\overline{F}_{ne}}{C_3^2 + C_4^2} \\ K_{rc} = \dfrac{C_2\overline{F}_{fc} + C_1\overline{F}_{nc}}{C_1^2 + C_2^2} & K_{re} = \dfrac{C_4\overline{F}_{fe} + C_3\overline{F}_{ne}}{C_3^2 + C_4^2} \\ K_{ac} = -\dfrac{\overline{F}_{ac}}{C_4} & K_{ae} = \dfrac{\overline{F}_{ae}}{C_5} \end{cases} \tag{29}$$

When the cutter's helix angle is equal to zero, the cutting zone will be $\phi_{st} \le \phi_j \le \phi_{ex}$; so, Eq. 29 can be simplified to Eqs. 30 and 31. The Eqs. 30 and 31 are the milling force coefficient formula without helix angle that has been studied in references [2, 18, 19, 21].

$$\begin{cases} K_{tc} = 4\dfrac{P\overline{F}_{fc} + Q\overline{F}_{nc}}{P^2 + Q^2} & K_{te} = -\dfrac{S\overline{F}_{fe} + T\overline{F}_{ne}}{S^2 + T^2} \\ K_{rc} = \dfrac{PK_{tc} - 4\overline{F}_{fc}}{Q} & K_{re} = \dfrac{SK_{te} + \overline{F}_{fe}}{T} \\ K_{ac} = \dfrac{F_{ac}}{T} & K_{ae} = -\dfrac{2\pi}{aN_f}\dfrac{\overline{F}_{ae}}{\phi_{ex} - \phi_{st}} \end{cases} \tag{30}$$

where

$$\begin{cases} P = \dfrac{aN_f}{2\pi}[\cos 2\phi]_{\phi_{st}}^{\phi_{ex}} & Q = \dfrac{aN_f}{2\pi}[2\phi - \sin 2\phi]_{\phi_{st}}^{\phi_{ex}} \\ T = \dfrac{aN_f}{2\pi}[\cos\phi]_{\phi_{st}}^{\phi_{ex}} & S = \dfrac{aN_f}{2\pi}[\sin\phi]_{\phi_{st}}^{\phi_{ex}} \end{cases} \tag{31}$$

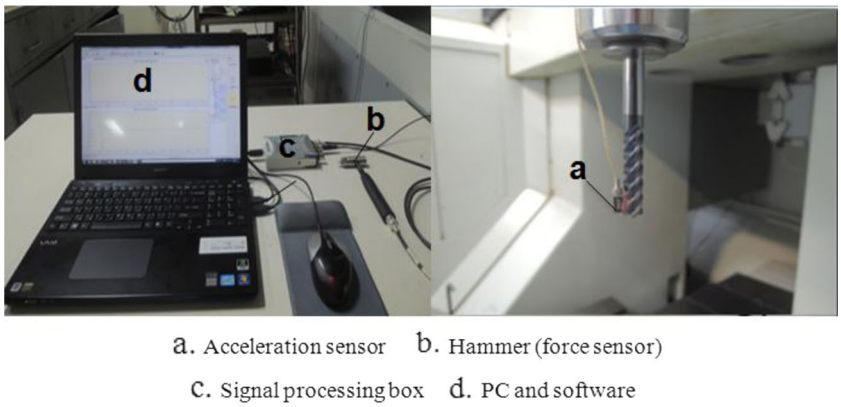

Fig. 6 Setup of experiment for analytical stability lobes

3 Experimental work

3.1 Experimental procedure

The research procedure was performed consisting of five steps that were carried out sequentially as shown in Fig. 5. In the step 1, the stable cutting condition was determined. First, the stability lobe diagram was measured by the CUTPRO™ software. By this work, the cutting depths and spindle speeds were selected in the stable zone of the stability lobe diagram. In the stable zone of the stability lobe diagram, the cutting tests avoided the chatter. And then, the stable cutting condition was chosen by testing the effect of cutting depth and spindle speed on the degree of variation of cutting force's amplitudes. Using this method, the effect of vibration and other factors on milling process was reduced. The detail of step 1 is explained in Sect. 3.2. In the step 2, the cutting tests were conducted to determine the cutting force coefficients. The detail of this step is described in Sect. 3.3. The cutting force coefficients were calculated from the experimental data, and the cutting forces were simulated by using the calculated cutting force coefficients. These are the works in step 3. In the step 4, the simulated cutting forces were verified by the experimental results. Finally, in step 5, the applications of the cutting force model and the cutting force coefficient data were proposed and performed.

3.2 Setup for determination of stable conditions in stability lobe zone

In order to determine the cutting force coefficients and verify the force model, a series of end milling experiments were performed. The cutter and workpiece were chosen as follows. Cutter: a carbide flat-end mill with number of flutes N_f=2, helix angle β=30°, rake angle α_r=5°, and the diameter was 8 mm. The workpiece material was Al6061-T6, and its compositions are listed in Table 1. The properties of the Al6061-T6 were the following: hardness 95 HB, Young's modulus= 68.9 GPa, Poisson's ratio=0.33, tensile strength=310 MPa. The experiments were performed at a Three-axis Vertical Milling Center (DECKEL MAHO–DMC70V hi-dyn).

An integrated device system that consisted of the acceleration sensor (ENDEVCO-25B-10668), hammer (KISTLER-9722A2000), signal processing box (NI 9234), and CUTPRO™ software was used to analyze the stability lobe. The detail setting of the measurement experiment is illustrated in Fig. 6.

Fig. 7 Setup measurement of cutting force setting

Table 2 Testing the most suitable machining condition

Test no.	Tool diameter [mm]	Number of flutes	Helix angle [deg]	Axial depth of cut [mm]	Feedrate [mm/tooth]	Spindle speed [rpm]
1	8	2	30	0.4	0.06	1000
2	8	2	30	0.4	0.06	3000
3	8	2	30	0.4	0.06	5000
4	8	2	30	1.2	0.06	1000
5	8	2	30	2.0	0.06	1000

The spindle speed and axial depth of cut in the stable zone were chosen according to the stability lobe diagram measured by CUTPRO^{TM} software as shown in Fig. 8. In addition, the selected point is the point in which the degree of variation of cutting force's amplitude is small. With this approach, a series of half-down milling tests were performed. The parameters of cutting condition are shown in Table 2. First, the cutting tests were performed with the variation of spindle speed. In this case, the values of spindle speed were 1000, 3000, and 5000 rpm. And then, the cutting tests were performed with the variation of cutting depth (0.4, 1.2, and 2.0 mm). The measured results of these tests were presented in Sect. 4.1.

3.3 Setup and measurement of cutting forces

A dynamometer (type XYZ FORCE SENSOR, model 624-120-5KN), signal filter and processing system, and a PC were used to measure cutting forces. The detail is illustrated in Fig. 7. At each depth of cut, half-down immersion experiments were repeated in every feedrate. The spindle speed was held constant at each experiment. The experiments were performed with the different parameters, as shown in Table 3.

4 Experimental results and discussion

4.1 The suitable machining conditions for determination of cutting force coefficients

Determination of the stable cutting condition is very important in the improvement of calculation accuracy of cutting force coefficients. Using the measured results of the frequency response function of the tool machine dynamic system, the stability lobes were analyzed by CUTPRO^{TM} software and described in Fig. 8. The stable cutting conditions (axial depth of cut and spindle speed) were chosen at the stable zone (color zone) of the stability lobe diagram.

The analysis results about the stability lobes show that the machining processing is stable at less than 2.0 mm of cutting depth, and at all range spindle speeds. In this zone, the chatter was prevented for all cutting tests. In fact, the effect of vibration, deflection, and other factors on the accuracy of the determined cutting force coefficients depends on the stability of measured cutting force. The experimental results showed that the spindle speed and the axial depth of cut affect strongly on the stability of cutting forces. A term called the degree of variation of cutting force's amplitude (Δ_q) was calculated to evaluate the effect of spindle speed and axial cutting depth on the stability of cutting force. It can be calculated by Eq. 32.

$$\Delta_q = \frac{A_q(\mathrm{Max}) - A_q(\mathrm{Min})}{A_q(\mathrm{Max})} * 100 \quad (q = f,\ n,\ a) \tag{32}$$

The effect of axial depth of cut and spindle speed on the degree of variation of cutting force's amplitude are illustrated in Figs. 9 and 10. The calculated results show that the cutting force's amplitudes change depending on the spindle speed and

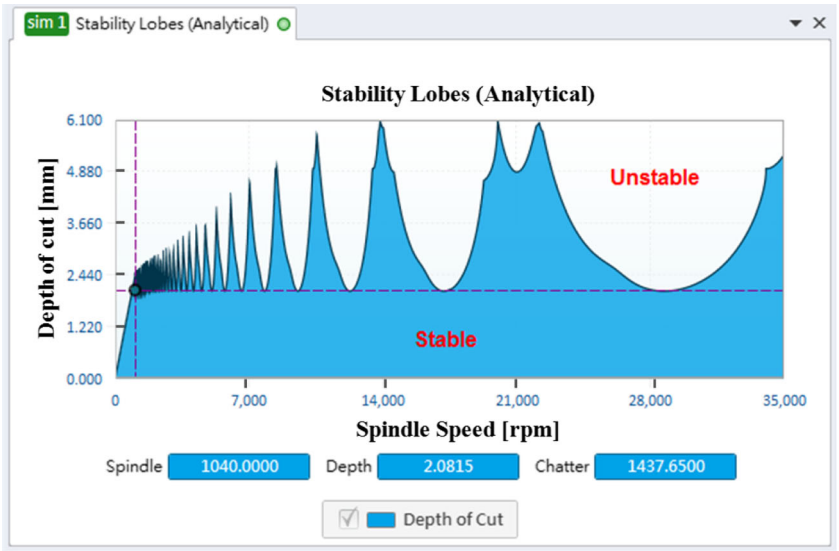

Fig. 8 The stability lobe diagram of the adopted CNC machine

Table 3 Testing the linear model force

Test no.	Tool diameter [mm]	Number of flutes	Helix angle [deg]	Axial depth of cut [mm]	Feedrate [mm/tooth]	Spindle speed [rpm]
1	8	2	30	0.4	0.02	1000
2	8	2	30	0.4	0.04	1000
3	8	2	30	0.4	0.06	1000
4	8	2	30	0.4	0.08	1000

axial depth of cut. For all cutting forces, the degrees of variation of cutting force's amplitudes increase with the increasing of the spindle speed. The conclusion is the same with the axial depth of cut. So, the smaller spindle speed or axial depth of cut is, the more stable cutting force is. The obtained results also show that the most suitable cutting condition (stable cutting condition) for determination of cutting force coefficients is 0.4 mm of axial cutting depth and 1000 rpm of spindle speed. This is the cutting condition that the degree of variation of cutting force's amplitude is the smallest in the stable cutting conditions. It means that, with this cutting condition, the effect of vibration and other factors (noise, deflection, and so on) on the calculation accuracy of the cutting force coefficient is the smallest. By this experimental method, the stable machining condition was determined to estimate the cutting force coefficients for each pair of cutter and workpiece in milling processes.

4.2 Verification on the linear model of average cutting forces

The cutting tests were performed at stable cutting conditions as listed in Table 3. For each experiment, the average cutting force in feed, normal, and axial directions were calculated from the measured cutting force data. The relationship of the average cutting force and the feedrate was estimated and illustrated in Fig. 11. In this figure, all the absolute values of average cutting forces increase with the increasing of feedrate. This experimental result is reasonable with the theory of cutting force model because when the feedrate increases towing, the chip thickness increases. The chip thickness increases make the cutting force's amplitude increase, and finally, the absolute value of average cutting force increases. The theoretical linear force model that was expressed by Eq. 28 is illustrated as these dash lines as shown in Fig. 11, the solid lines are the experimental results of the linear force model, and in each direction, the solid line is very close to the dash line. The verified results show that the theory results and experimental results have good agreement, and the relationship of average cutting forces and feedrate is close to the linear function. Therefore, in cylindrical flat-end mill with stable cutting condition (no chatter and very small vibration, etc.), the measured average cutting force can be expressed by the linear function of feedrate as expressed by Eq. 28, and the measured data can be used to estimate the cutting force coefficients for each pair of cutter and workpiece. By this method, all cutting force coefficient components were determined.

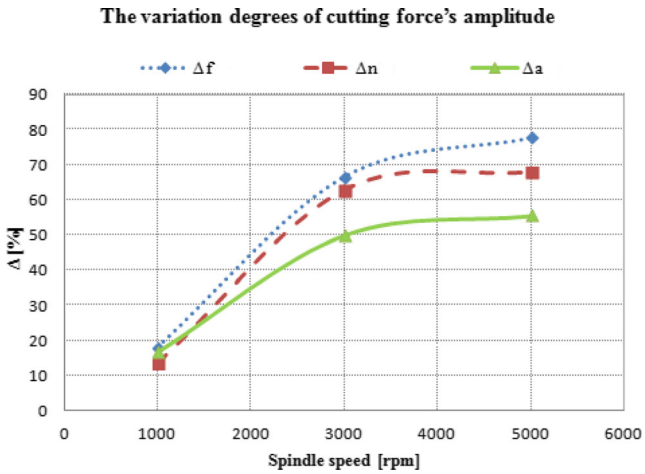

Fig. 9 The degree of variation of cutting force's amplitude versus spindle speed

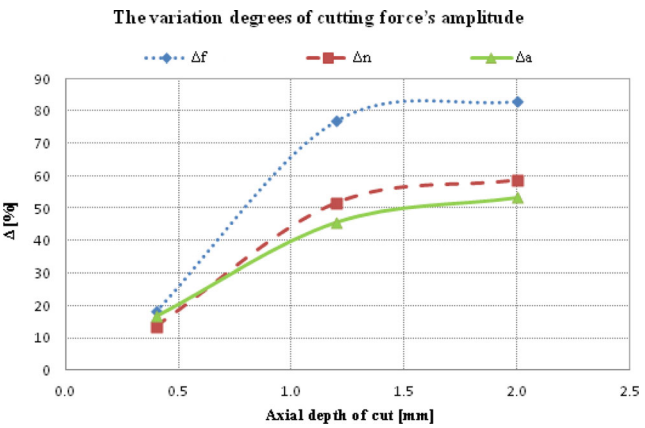

Fig. 10 The degree of variation of cutting force's amplitude versus cutting depth

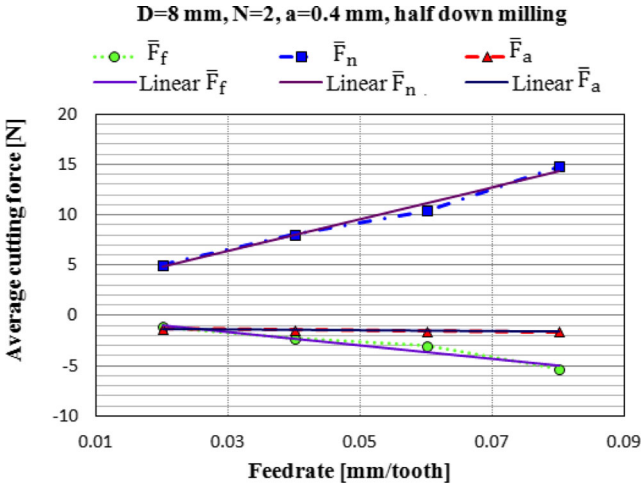

Fig. 11 The average cutting forces versus feed rate

4.3 Determination of cutting force coefficients by experimental data

Using Fitting Toolbox of MATLAB™ and linear regression, the best lines passing through the values of average cutting forces were determined. Considering Eqs. 26 to 29 and using the characteristic of the best line, the cutting force coefficients were calculated and listed in Table 4. The calculated results of cutting force coefficients with the cutter's helix angle (research model) were compared with the calculated results without the cutter's helix angle (simplified model). The absolute values of cutting force coefficients between the research model and the simplified model were different. With each cutting force coefficient, the absolute value of cutting force coefficient in research model is larger than that one in the simplified model. In this case, the maximum difference is about 17.285 %, and minimum difference is about 2.442 %. The main reason of the differences is that when determining the cutting force coefficients, the effect of cutter's helix angle was considered in the research model but was not considered in the simplified model. The above research results show that the cutter's helix angle plays a highly significant factor for determination of cutting force coefficients. So, when building the model to calculate the cutting force coefficients, the cutter's helix angle should be considered. The results in Table 4 also show that the important cutting force coefficients are the shearing force coefficients because the absolute values of shearing force coefficients are more times as large as absolute values of edge force coefficients.

4.4 Verification of simulation results

Using the calculated cutting force coefficients by two ways, with and without the cutter's helix angle, the cutting forces were predicted and compared with the measured results. The predicted cutting forces have a little difference to the measured cutting forces, as shown in Fig. 12. In all directions (feed, normal, and axial), the amplitude of the simulated force with the cutter's helix angle is larger than that one of measured force and predicted force without the cutter's helix angle. The predicted results of cutting force are different in research model and in the simplified model because in the calculation of cutting force coefficients, the cutter's helix angle was considered in the research model, but it was neglected in the simplified model, and so, the absolute value of cutting force coefficient in the research model is larger than that one in the simplified model as explained in Sect. 4.3. Moreover, about the shape of measured forces and predicted forces, these differences are small. The reasons for the above differences were mostly originated from the noise, the vibrations, the deflection, the inconstancy of cutting depth, the inhomogeneous distribution of tool and workpiece hardness, the temperature, the friction, and so on. Although, the effect of factors (vibration, noise, temperature, etc.) is limited in the experiments, but in fact, this effect still exists in each experiment. Above all, the predicted results of research model are close to the experimental results, and these research results showed that the predicted results from research model agree satisfactorily with experimental results. Therefore, the cutting force models and cutting force coefficient models in this study are good models that can be used to determine the cutting force coefficients and predict the cutting force in milling processes.

Table 4 Prediction and comparison of cutting force coefficients

Model	Shearing force coefficient [N/mm^2]			Edge force coefficient [N/mm]		
	K_{tc}	K_{rc}	K_{ac}	K_{te}	K_{re}	K_{ae}
Research model	1467.640	274.782	−43.088	8.810	5.690	−6.907
Simplified model	1432.651	244.494	−41.820	7.768	4.706	−5.982
Different (%)	**2.442**	**12.388**	**2.941**	**11.828**	**17.285**	**13.392**

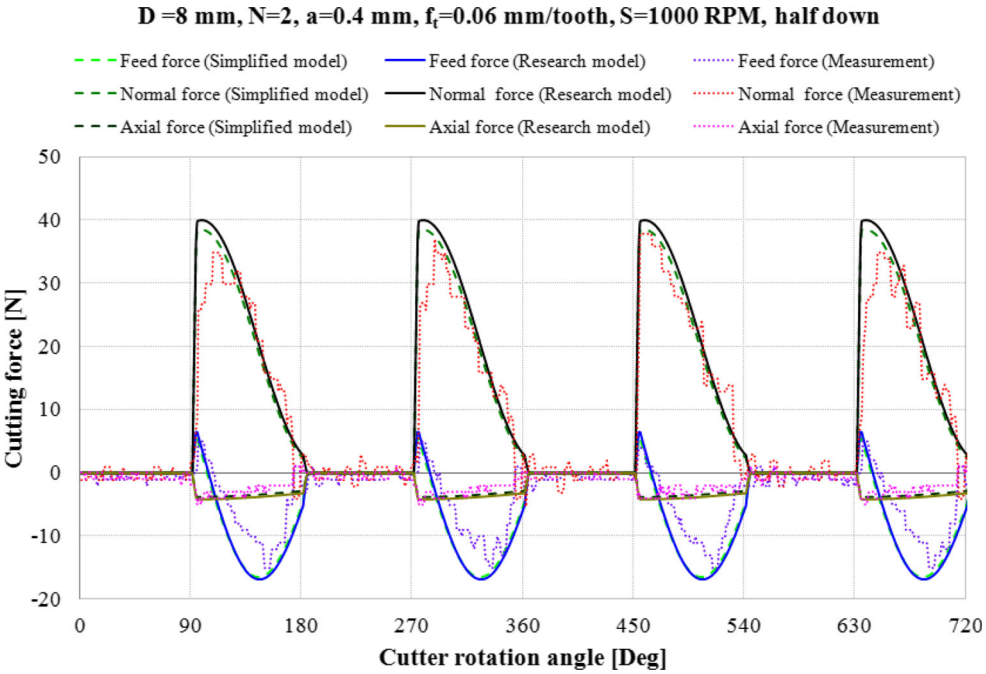

Fig. 12 Verification of simulation results

4.5 Application of the results

This study has successfully proposed a prediction method to determine the cutting force coefficients. The cutting forces could be simulated by the proposed force model with the consideration of the effect of the cutter's helix angle. The proposed method can be used to calculate the cutting force coefficients for each pair of different cutter and workpiece and is expected to be applied for the analysis of machine tool development, milling simulation, milling operation optimization, and the analysis of system stability.

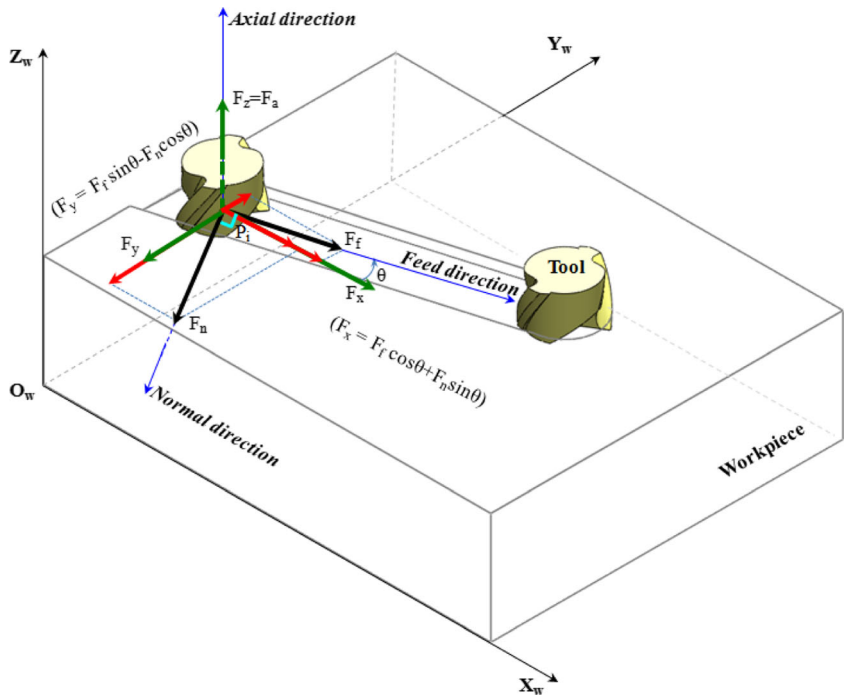

Fig. 13 Cutting forces in x, y, and z directions

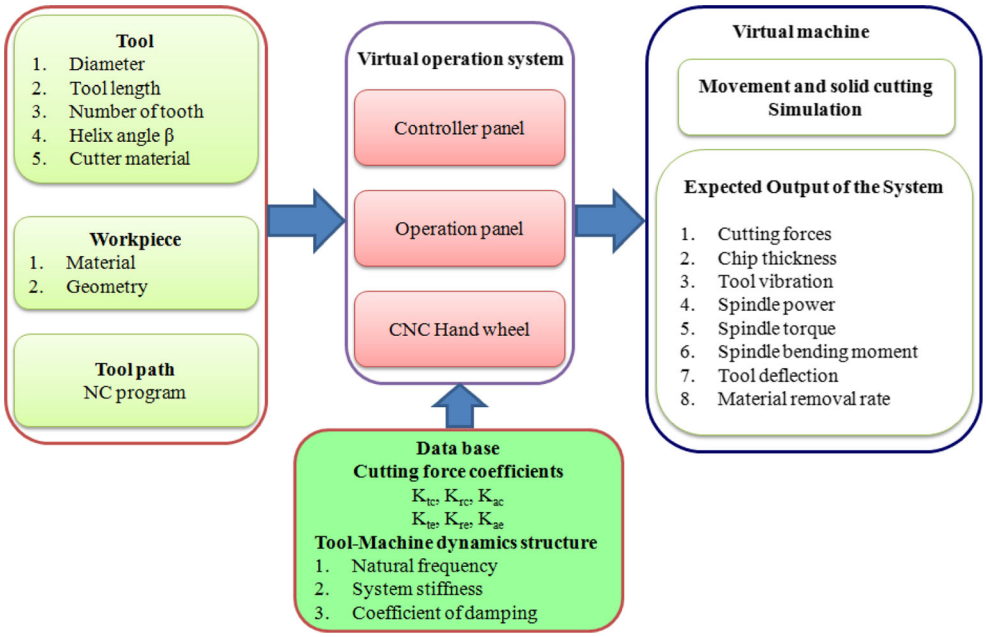

Fig. 14 The processing procedure of virtual vertical milling simulation system

For example, in three-axis milling machine center, the cutting forces in x, y, and z directions are illustrated as in Fig. 13 and can be expressed in Eq. 33 through the coordinate transformation.

$$\begin{Bmatrix} F_x \\ F_y \\ F_z \end{Bmatrix} = \begin{bmatrix} \cos\theta & \sin\theta & 0 \\ \sin\theta & -\cos\theta & 0 \\ 0 & 0 & 1 \end{bmatrix} \begin{Bmatrix} F_f \\ F_n \\ F_a \end{Bmatrix} \tag{33}$$

By investigation of several real CNC machine centers, and integration of software on graphic designing, 3D simulation, and programming, a virtual vertical milling simulation system (VVMS) was constructed by the authors to implement the proposed cutting force calculation model. The developed force calculation model has also been successfully integrated into this system as shown in Fig. 14. This system consists of virtual CNC machines, virtual CNC operation systems, and the cutting simulation part, etc. as shown in Fig. 15.

This VVMS system is used as an application installed in a personal computer running Microsoft Windows Operating System, which the virtual machine, virtual operation system, and the virtual CNC hand wheel can be operated in emulating a real CNC machining system. In this integrated system, the cutting force coefficients were determined through cutting experiments and were stored into the database. To calculate the cutting forces, the related input parameters include the tool geometry, tool material properties, workpiece geometry, workpiece material properties, and the machining conditions. The machining conditions such as "depth of cut," "spindle speed," and "feedrate" are obtained and calculated from NC program and workpiece properties. From these parameters, this integrated system can dynamically calculate and display the cutting forces during solid cutting simulation.

5 Conclusions

In this study, the linear force model was adopted to determine the cutting force coefficients in considering the effect of cutter's helix angle. The developed model was used to analyze the theory of calibrating the cutting force coefficients with a series of milling tests. This has resulted in an improved theoretical model to be proposed with an effective model for the determination of cutting force coefficients. This method could be applied in the stable cutting condition when the machine tool vibration is small and the effects of other subordinate factors are limited.

An experimental method to determine the stable cutting condition was proposed. By this method, the chatter was prevented, and the effect of vibration and other factors on the accuracy of calculation cutting force coefficients was reduced in the milling process. The

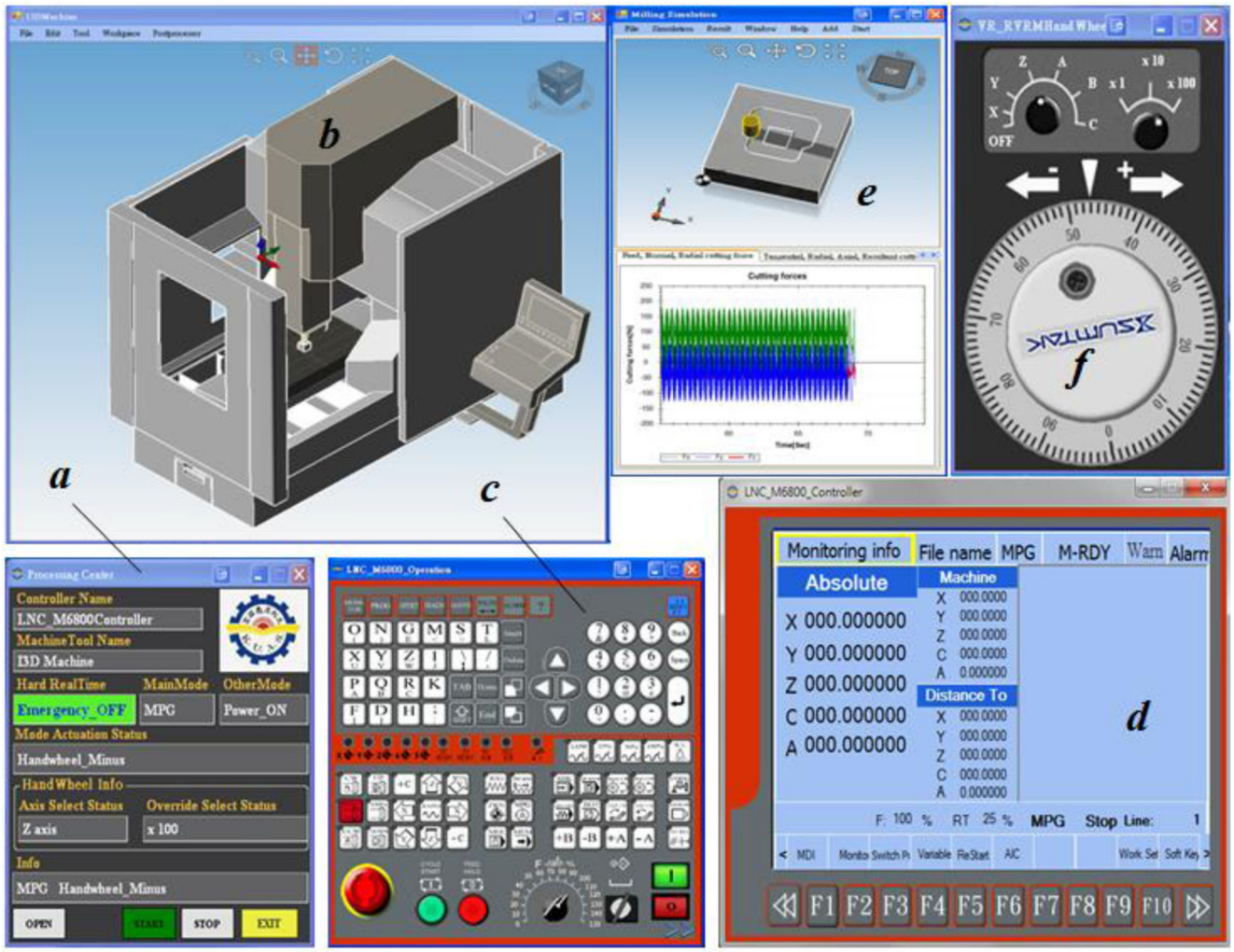

(a) Processing center (b)Virtual vertical milling machine center (c) Operation panel

(d) Controller panel (e) Solid cutting simulation showing cutting forces (f) Hand wheel

Fig. 15 Application of cutting force model in a virtual vertical milling simulation system

degree of variation of cutting force's amplitude was estimated to analyze the stability of cutting force. The cutting condition in which the degree of variation of cutting force's amplitude is the smallest is the stable cutting condition. This is the most suitable cutting condition to perform the cutting tests for determination of the cutting force coefficients. This method can be applied to determine cutting force coefficients for each pair of cutter and workpiece.

In the stable cutting condition, the average cutting forces were close to a linear function of feedrate, and the cutter's helix angle has a highly significant effect on the calculation of cutting force coefficients. The verified results also showed that the predicted and measured results had a good agreement with both the amplitude and the shape of cutting forces. By the model proposed in this paper, all cutting force coefficients were determined by experimental data.

This research model is suitable for cylindrical flat-end mill, and it can be applied to a wide range of cutter and workpiece properties. On the other hand, this model also can be extended to more complex type of milling tool such as ball-end mill, bull-end mill, and general-end mill. Moreover, the application of the developed research model had been successfully integrated into a virtual vertical milling center simulation system. The integrated system is expected to have potential application for education, training, manufacturing simulation, and will be the futuristic study of the extended research.

Acknowledgments The authors appreciate the support from the grant NSC 102-2218-E-151-007 and the generous assistance from the High Speed Machining Lab for the dynamometer in the cutting forces

measurement experiments. Thanks also extend to the support from the Advanced Institute of Manufacturing with High-tech Innovations, National Chung Cheng University, Taiwan.

References

1. Merchant ME (1945) Mechanics of the Metal Cutting Process. I. Orthogonal Cutting and a Type 2 Chip. J Appl Phys 16:267. doi:10.1063/1.1707586
2. Altintas Y (2012) Manufacturing automation: metal cutting mechanics, machine tool vibrations, and CNC design, 2nd edn. Cambridge University Press, New York, ISBN 978-1-00148-0
3. Fernández-Abia AI, Barreiro J, López de Lacalle LN, Martínez-Pellitero S (2012) Behavior of austenitic stainless steels at high speed turning using specific force coefficients. Int J Adv Manuf Technol 62:505–515
4. Guibert N, Paris H, Rech J (2008) A numerical simulator to predict the dynamical behavior of the self-vibratory drilling head. Int J Mach Tools Manuf 48:644–655
5. Budak E, Altintas Y, Armarego EJA (1996) Prediction of milling force coefficients from orthogonal cutting data. ASME J Manuf Sci Eng 118:216–224
6. Sonawane HA, Joshi SS (2010) Analytical modeling of chip geometry and cutting forces in helical ball end milling of superalloy Inconel 718. CIRP J Manuf Sci Technol 3:204–217
7. Li XP, Li HZ (2004) Theoretical modelling of cutting forces in helical end milling with cutter runout. Int J Mech Sci 46:1399–1414
8. Yang M, Park H (1991) The prediction of cutting force in ball-end milling. Int J Mach Tools Manuf 31:45–54
9. Lee P, Altintas Y (1996) Prediction of ball-end milling forces from orthogonal cutting data. Int J Mach Tools Manuf 36:1059–1072
10. Budak E, Ozturk E, Tunc LT (2009) Modeling and simulation of 5-axis milling processes. CIRP Ann Manuf Technol 58(1):347–350
11. Cheng PJ, Tsay JT, Lin SC (1997) A study on instantaneous cutting force coefficients in face milling. Int J Mach Tools Manuf 37:1393–1408
12. Bayoumi AE, Yucesan G, Kendall LA (1994) An analytic mechanistic cutting force model for milling operations: a theory and methodology. Trans ASME J Eng Ind 116:324–330
13. Shin YC, Waters AJ (1997) A new procedure to determine instantaneous cutting force coefficients for machining force prediction. Int J Mach Tools Manuf 37:1337–1351
14. Larue A, Anselmetti B (2003) Deviation of a machined surface in flank milling. Int J Mach Tools Manuf 43:129–138
15. Azeem A, Feng HY, Wang L (2004) Simplified and efficient calibration of a mechanistic cutting force model for ball-end milling. Int J Mach Tools Manuf 44:291–298
16. Ko JH, Cho DW (2005) Determination of cutting-condition-independent coefficients and runout parameters in ball-end milling. Int J Adv Manuf Technol 26:1211–1221
17. Subrahmanyam KVR, San WY, Soon HG, Sheng H (2010) Cutting force prediction for ball nose milling of inclined surface. Int J Adv Manuf Technol 48:23–32
18. Altintas Y (2000) Modeling approaches and software for predicting the performance of milling operations at MAL-UBC. Int J Mach Sci Technol 4(3):445–478
19. Budak E (2006) Analytical models for high performance milling. Part I: cutting forces, structural deformations and tolerance integrity. Int J Mach Tools Manuf 46:1478–1488
20. Adetoro OB, Wen PH (2010) Prediction of mechanistic cutting force coefficients using ALE formulation. Int J Adv Manuf Technol 46:79–90
21. Wang M, Gao L, Zheng Y (2014) An examination of the fundamental mechanics of cutting force coefficients. Int J Mach Tools Manuf 78:1–7
22. Compeán FI, Olvera D, Campa FJ, López de Lacalle LN, Elías-Zúñiga A, Rodríguez CA (2012) Characterization and stability analysis of a multi variable milling tool by the enhanced multistage homotopy perturbation method. Int J Mach Tools Manuf 57:27–33
23. Wan M, Zhang WH, Qin GH, Tan G (2007) Efficient calibration of instantaneous cutting force coefficients and runout parameters for general end mills. Int J Mach Tools Manuf 47:1767–1776
24. Wan M, Lu MS, Zhang WH, Yang Y (2012) A new ternary-mechanism model for the prediction of cutting forces in flat end milling. Int J Mach Tools Manuf 57:34–45
25. Dang JW, Zhang WZ, Yang Y, Wan M (2010) Cutting force modeling for flat end milling including bottom edge cutting effect. Int J Mach Tools Manuf 50:986–997
26. Wan M, Zhang WH, Dang JW, Yang Y (2010) A novel cutting force modeling method for cylindrical end mill. Appl Math Model 34:823–836
27. Bhattacharyya A, Schueller JK, Mann BP, Ziegrt JC, Schmitz TL, Taylor FJ, Fitz-Coy NG (2010) A closed form mechanistic cutting force model for helical peripheral milling of ductile metallic alloys. Int J Mach Tools Manuf 50:538–551
28. Perez H, Diez E, Marquez JJ, Vizan A (2013) An enhanced method for cutting force estimation in peripheral milling. Int J Adv Manuf Technol 69:1731–1741
29. Wang B, Hao H, Wang M, Hou J, Feng Y (2013) Identification of instantaneous cutting force coefficients using surface error. Int J Adv Manuf Technol 68:701–709
30. Liu XW, Cheng K, Webb D, Luo XC (2002) Improved dynamic cutting force model in peripheral milling. Part I: theoretical model and simulation. Int J Adv Manuf Technol 20:631–638
31. Narita H (2013) A determination method of cutting coefficients in ball end milling forces model. Int J Autom Technol 7(1):39–44
32. Tukora B, Szalay T (2011) Real-time determination of cutting force coefficients without cutting geometry restriction. Int J Mach Tools Manuf 51:871–879
33. Gao G, Wu B, Zhang D, Luo M (2013) Mechanistic identification of cutting force coefficients in bull-nose milling process. Chin J Aeronaut 26(3):823–830
34. Gradišek J, Kalveram M, Weinert K (2004) Mechanistic identification of specific force coefficients for a general end mill. Int J Mach Tools Manuf 44:401–414